

# Fabrication And Characterization Of Magnetoresponseive Carbon Nanotube Infused Polysulfone Nanocomposites

Shisia K. Silvanus

Department of Chemistry,  
Kenyatta University, Kenya

Andala M. Dickson

Department of Chemistry,  
MultiMedia University of Kenya

**Abstract:** Many attempts have been made to fabricate various types of inorganic nanoparticle-filled polymers by a mechanical or chemical approach. However, these approaches require modification of the nanofiller surfaces and/or complicated polymerization reactions, making them unsuitable for industrial-scale production of the nanocomposites. This work investigated the potential of magnetoresponseive CNT-polysulfone infused polymeric nanocomposites (CNT-IPSF/Fe<sub>3</sub>O<sub>4</sub>) for water purification against PAHs and heavy metals pollution. The CNTs with internal diameters of 40-50 nm were prepared by chemical vapour deposition (CVD) process. Magnetite and silica coated magnetite nanoparticles (NPs) prepared by solvothermal and sol gel methods respectively exhibited UV spectra with absorption peaks at about 396 nm and 395 nm respectively. The presence of absorption band in IR spectrum at 580 cm<sup>-1</sup> was assigned to the vibrations of Fe-O bond confirming the formation of Fe<sub>3</sub>O<sub>4</sub> nanoparticles. The XRD analysis of NPs showed strongest peak at D(311) plane, characteristic of a cubic spinel structure (JCPDS No. 82-1533). The SQUID magnetometry of the prepared magnetite silica NPs obtained displayed a thin hysteresis loop with magnetization of 2.0 emu/g.

**Keywords:** magnetoresponseive; nanocomposite; silica nanoparticle; agglomerate; packing arrangement; fabrication; characterization; surface morphology; magnetic property.

## I. INTRODUCTION

Due to recent developments in the field of nanotechnology, there has been growing interest in polymer-matrix composites in which nano-sized fillers are distributed homogeneously due to their unique optical, electric and magnetic properties, as well as their dimensional and thermal stability [1]. The traditional practical method for dispersing inorganic nanofillers in polymer matrices is direct melt-compounding of the polymer with the fillers [2]. However, the surface activity of the nanofillers is extremely high, and the particles consequently have a tendency to aggregate tightly, creating micron-sized filler-clusters. A number of attempts have shown possibility of dispersing nanoparticles uniformly into polymer matrices by using methods with organic modification of the surface and a variety of sol-gel and/or polymerization reactions. However, these technologies require complicated chemical reactions making them unsuitable for industrial-scale production of nanocomposites with a wide

volume fraction range of nanoparticles and various combinations of nanoparticles and polymer material species.

Adsorbents such as activated charcoal, silica gel, and zeolites are commonly used in industries for the removal of water pollutants, which include toxic metals [3]. Most of these adsorbents are synthetic and have been popularly used in water-treatment processes. However, investigations into their use as biosorbents have recently gained momentum because of environmental and cost considerations. The literature reveals that carbon nanotubes are good adsorbents and modification of their outer surfaces followed by dispersibility in polysulfone (through hydrogen bonding) provide suitable functional groups (-COOH, -OH and -SH) which are capable of ionizing in suitable solvents, thereby providing charged functionalities that could scavenge toxic metal ions through cation exchange [4].

In recent years, much attention has been focused on the synthesis of uniformly sized magnetic nanoparticles [5]. However, most of these nanoparticles have been synthesized

in organic solvents using hydrophobic capping reagents. The resulting magnetic nanoparticles are dispersible in hydrophobic organic solvents. However, the biological applications of these nanoparticles are greatly restricted because of their poor dispersibility in aqueous media and membrane biofouling. Very recently, there have been several reports on the synthesis of water dispersible magnetic nanoparticles [6], in which magnetic nanoparticles are functionalized with water-compatible chemical reagents. Silica surfaces are biocompatible and can be easily functionalized for bio-conjugation purposes. Because of these advantages, magnetic-silica composite nanoparticles with various shapes (spheres, rods, and plates) have been synthesized. However, the magnetic nanoparticles obtained showed ferromagnetic behavior, which causes a remanent magnetization problem when the applied magnetic field is removed. Super-paramagnetic nanoparticles are desirable as the magnetic hosts need to be easily dispersed after each magnetic separation. To obtain silica-coated superparamagnetic nanoparticles with more versatile applications, it would be desirable to synthesize uniformly sized magnetite-silica nanoparticles via a simple and easy synthetic route and embed them into polymeric structures so that the nanocomposite exhibit magnetoresponsive property.

To our knowledge, there have been no reports on the simple synthesis of discrete, uniformly sized magnetic-nanoparticle-core/silica-shell superpara-magnetic nanoparticles embedded into polymeric carbon nanotube-infused polysulfone matrix. Herein, we report on the novel synthesis of magnetite-silica nanoparticles by the simple addition of tetraethyl ortho-silicate (TEOS), dispersing into CNT-IPSF solution and finally casting the solution to form the nanocomposite membrane.

## II. EXPERIMENTAL SECTION

**MATERIALS FOR CNTS SYNTHESIS:** Iron powder, ethylene gas, argon gas, flow rate meters were purchased from Aldrich (Milwaukee, WI), and N,N-dimethylformamide (DMF) were purchased from Sigma (St Louis, MO). All other reagents and solvents were purchased from Aldrich (Milwaukee, WI, USA), and were of the highest grade commercially available. Lindberg tube furnace was procured from Department of physics, Kenyatta University,

**METHOD:** A continuous chemical vapour deposition (CVD) reactor was used to produce CNTs at temperatures of 600 and 700°C as outlined in our previous studies. About 0.1g Fe powder on ceramic boat was placed in the standard fixed bed reactor furnace of Lindbergh tube furnace (Model TF55035C-1). Iron catalyst was chosen due to high solubility of carbon in the metal at high temperature (1500°C); high carbon diffusion rate in the metal and wide temperature window of CVD for wide range of carbon precursors. Iron powder was used in order to decrease average diameter of CNTs [7]. Ceramic boats were used as support for iron catalyst and also CNTs formed because they can withstand high temperatures.

The process involved passing acetylene hydrocarbon/argon at optimum flow rate of 8ml/min and 1

ml/min respectively through a tubular reactor for 30 mins to accurately measure acetylene conversion and the production yield. At this flow rate, argon could carry enough of the carbon sources (acetylene) into the reactor. Besides, with this rate, the carbon source has enough time for decomposition and deposition on the catalyst. The production of CNTs was varied at 600-700 °C since this is in the range of 600-900 °C which supports synthesis of MWCNTs.

**MATERIALS FOR MAGNETITE AND MAGNETITE-SILICA NANOPARTICLES SYNTHESIS:** Ethanol, ammonia, tetraethyl orthosilicate (TEOS), HCl, FeCl<sub>3</sub>·6H<sub>2</sub>O, ethylene glycol, sodium acetate and polyethylene glycol-200 were obtained from Sigma Aldrich Co. An 80 mL capacity Teflon lined stainless-steel autoclave, pH meter, vacuum oven and water bath were provided by the department of chemistry.

**METHOD:** Magnetic magnetite particles (MMP) were prepared via solvothermal reaction according to the method previously reported [8]. About 2.7 g FeCl<sub>3</sub>·6H<sub>2</sub>O was dissolved into 80 mL ethylene glycol to form orange transparent solution. Then 7.2 g sodium acetate and 2.0 ml polyethylene glycol-200 were added into the solution to form emulsion mixture under vigorous stirring for 30 minutes. Finally the emulsion was sealed into an 80 mL capacity Teflon lined stainless-steel autoclave, and maintained at 200 °C for 8 hours. The black MMP products were washed several times with ethanol and deionized water, and then immersed in HCl solution of pH 1 for 24 h. The MMP were washed with deionized water to neutral pH, and dried at room temperature in a vacuum oven.

Magnetite silica NPs were prepared by sol-gel approach [9]. About 0.1 g of the MMP were dispersed in 100 mL ethanol by ultrasonic vibration in water bath for 30 minutes, then 25 mL deionized water and 3.125 mL ammonia aqueous were added into ethanol dispersion under continuous mechanical stirring, followed by slow addition of 50 µL tetraethyl orthosilicate (TEOS). The mixture was kept stirred for 12 hours at room temperature, silica was formed on the surface of MMP through hydrolysis and condensation of TEOS, and MMP-Silica Microspheres (MMP-SM) were obtained. The MMP-SM product was washed several times with ethanol and deionized water, and then immersed in 1 M HCl for 24 hours to remove unwrapped MMP. The MMP-SM were then washed with water to neutral pH, and dried on glass plate at 60°C for 2 hours in a vacuum oven.

**CHARACTERIZATION OF THE MATERIALS:** The as-prepared CNTs were characterized by using SEM, TEM and EDAX for their size, morphology and elemental composition. The silica-coated magnetic nanoparticles were characterized by UV-Vis, IR, SEM, XRD and SQUID. TEM was performed on a Jeol EM-2010 microscope while XRD patterns were obtained with a Rigaku D/Max2500 diffractometer equipped with a rotating anode and a CuK $\alpha$  radiation source ( $\lambda=0.15418$  nm). The IR spectra were collected on spectrometers. The as-prepared magnetic CNT-IPSF were characterized using SEM-EDAX and TEM.

**FABRICATION AND CHARACTERIZATION OF MAGNETIC CNT-IPSFNANOCOMPOSITE:** The as-prepared CNTs produced were blended with PSF by a phase inversion method as per literature [10] with modification. A bout 0.1 g CNTs were mixed with 10 ml N, N-dimethylformamide

(DMF) with constant stirring. 5 g of PSF was also mixed separately with 50 ml DMF with stirring to make its solution at 50 °C. The two solutions were mixed with constant shaking in a shaking water bath at 50°C to make CNT-PSF solution. About 0.3g of magnetite silica NPs were added to CNT-PSF polymer solutions and the solutions ultrasonicated for 1 hour. The magnetite-CNT-IPSF polymer solutions were immediately cast onto a glass plate with the aid of an aspirator. The cast solution was left in ambient conditions for 10 min and thereafter fully immersed in distilled water for a period of 24 hours. Upon draining off the liquid, a 1% (w/v) aqueous polyvinyl alcohol (PVA) solution was poured over the membrane and kept in contact for 3 minutes. The membrane was then heated in an oven at 60°C for 30 minutes followed by overnight drying in ambient air. The structure of the membranes was characterized by SEM-EDAX and TEM techniques.

### III. RESULTS

#### A. CHARACTERIZATION OF CNTS

##### a. SCANNING ELECTRON MICROSCOPY

The SEM images of prepared CNTs are shown (Fig.1a). This SEM image shows the configuration of the as-prepared material with abundant threadlike entities clearly seen. The SEM images further provide evidence that the twisting and winding entities are for MWNTs.

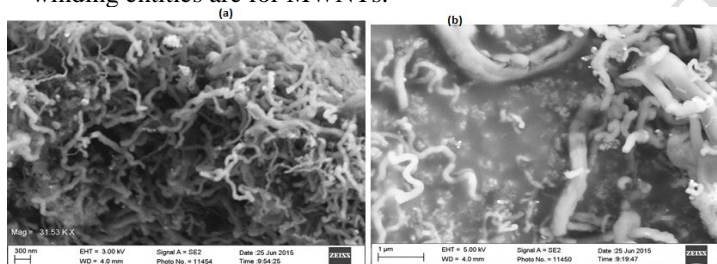


Figure 1: SEM images of CNTs at different magnifications

It is difficult to make out the accurate length of the MWNTs from the SEM observation due to the twisting, but the length could be more than several tens of micrometers from the enlarged image (Fig. 1 b).

##### b. TRANSMISSION ELECTRON MICROSCOPY (TEM)

As shown in Figure. 2, the enlarged image show that the MWNTs are about 40–60 nm in their outer diameter. Based on the preparation procedure, the typical impurity in the as-grown specimen is the catalyst; which is distributed at the black spot on the nanotube.

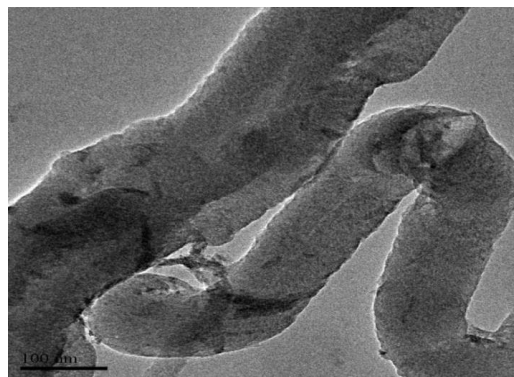


Figure 2: HRTEM of as-grown CNTs

Based on the preparation procedure, the few black areas are possibly due to agglomerated catalyst particles. The typical impurity in the as-grown specimen is the iron catalyst.

##### c. ENERGY DISPERSIVE SPECTRUM (EDS)

The area marked and shown with an arrow in Fig. 3a was analyzed by EDAX and the EDS result is shown in Fig. 3b. Elements Fe, Si and O were detected and their weight ratios accord with the catalyst component. This confirms that the above guess is reasonable, that is, the black points observed in Fig. 3 are for Fe, Si, catalyst particles. Thus, the dominant impurity in the as grown material was the Fe and Si catalysts.

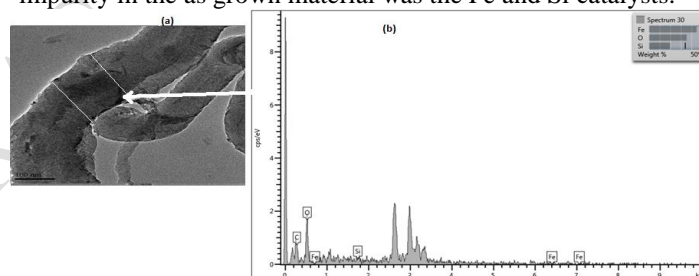


Figure 3: EDS analysis of selected part of MWNTs

The presence of C and O atoms could signify oxidation by  $\text{HNO}_3$  used during purification process which may have led to  $-\text{COO}-$  on the CNTs.

It can be seen from the Fig. 3a that the tips of the our MWCNTs were closed, which is a feature of unmodified MWCNTs before purification. After possible purification (Fig. 4), however, the end tips of many MWCNTs were opened, indicating the breaking of the C=C bond along the graphene layers of the co-axial tubes [11]. The layered structure of the MWCNTs remained largely intact, which indicates that there was no real damage to the MWCNTs during the oxidation process.

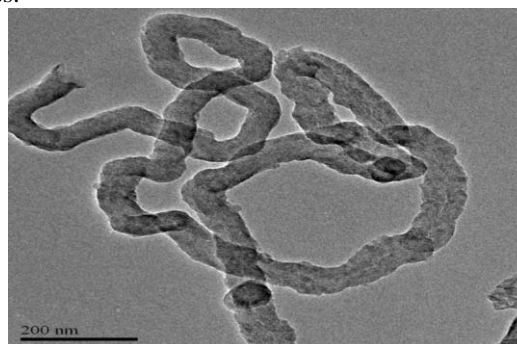


Figure 4: TEM for purified MWCNTs

## B. CHARACTERIZATION OF MAGNETITE AND MAGNETITE-SILICA NPS

### a. UV-VIS SPECTROMETRY

The UV-Vis spectrum for magnetite and magnetite silica NPs is shown in Figure 5.

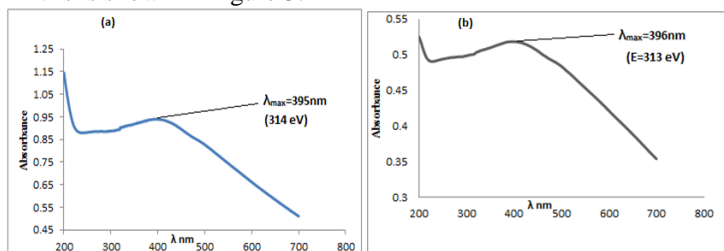


Figure 5: UV-Vis for magnetite NPS (a)  $Fe_3O_4$  and (b)  $Fe_3O_4.SiO_2$

UV-Vis absorption was the first characterization technique for prepared nanoparticles, to check whether the prepared sample was in nano range or not as it gives information about formation of nanoparticles, the band-gap energy, and its size distribution from the absorption spectrum. Absorbance of magnetite and magnetite silica nanoparticles obtained as in the spectra (Figure 5 a, b) were calculated using digital spectrometer at 396 nm for magnetite and 395 nm for silica coated magnetite NPs. By putting the respective values in the famous Einstein-plank's relation ( $E = \frac{hc}{\lambda}$ ), the obtained energy of band gap was 3.13 and 3.14 eV for (a) magnetite NPs and (b) magnetite silica NPs syntheses at wavelength, 396 nm and 395 nm respectively. The UV-Vis spectroscopy revealed that the material has turned into nanoparticle form showing enhancement in band gap energy in magnetite silica NPs, which is higher than the corresponding magnetite NPs [12]. The results obtained, proved that the particles synthesized were in quite stable and in nano range.

It can be observed that with addition of TEOS content, the absorption peak is shifted towards the higher wavelength side i.e. shift from figure 5a to 5b is observed. With the increase in particle size the band gap energy of a material decreases which results in the shifting of the absorption peak towards the higher wavelength side. This phenomenon occurs; since in a nanomaterial the energy levels are discretely defined and the energy level shifts according to the quantum size effect (QSE) but when the size of the particle increases the energy levels is no longer discrete which decreases the band gap energy of the material. In the present study it is observed that with the addition of TEOS content in the composite, the particle size of the composite was found to increase and hence the band gap energy decreased [13].

### b. FOURIER TRANSFORM INFRARED (FTIR) SPECTROSCOPY

FT-IR spectroscopy is cheaper than other conventional spectroscopic methods and also measures information at all frequencies simultaneously. An infrared spectrum (Figure 6) was obtained by passing IR radiation through the sample pellet, which determined the maximum fraction of incident

radiation absorbed at a particular energy. The absorption was in the range of  $1500-4000\text{ cm}^{-1}$  corresponding to the face centered cubic crystal. The main absorption peak is at  $\sim 1500-2000\text{ cm}^{-1}$  ( $\sim 2981 \times 10^{-25} - 3975 \times 10^{-25}\text{ J}$ ).

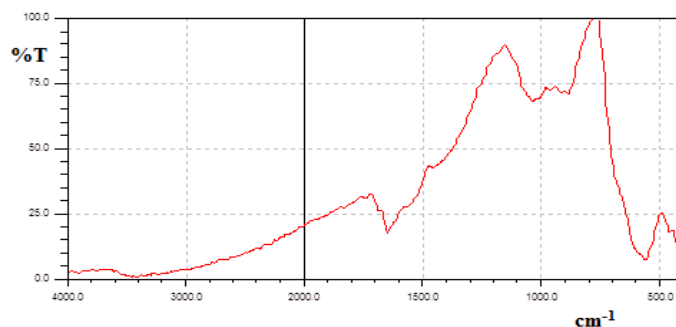


Figure 6: FT-IR spectrum for magnetite-silica NPs synthesized

The presence of absorption band between  $480\text{ cm}^{-1}$  and  $580\text{ cm}^{-1}$  is assigned to the vibrations of Fe-O bonding in  $Fe_3O_4$  nanoparticles. Previously, it was reported that the characteristic absorption band for Fe-O in bulk  $Fe_3O_4$  appeared at 570 and  $400\text{ cm}^{-1}$  wave number. However, in the present case the band for Fe-O shift towards higher wave number of  $580\text{ cm}^{-1}$  due to the breaking of the large number of bands on the surface atoms, resulting in rearrangement of localized electrons on the particle surface. The surface bond force constant also increases as  $Fe_3O_4$  is reduced to nanoscale range, hence the absorption bands shift to higher wave number [14].

### c. SCANNING ELECTRON MICROSCOPY (SEM)

The SEM micrographs of the magnetite ( $Fe_3O_4$ ) and silica modified magnetite ( $Fe_3O_4.SiO_2$ ) nanoparticles are shown in Fig. 7a and b respectively. It was found that with the addition of TEOS content, clear and distinct spherical shaped particles were obtained. It can also be seen that the particle shape is improved with the addition of TEOS content (Fig. 7b).

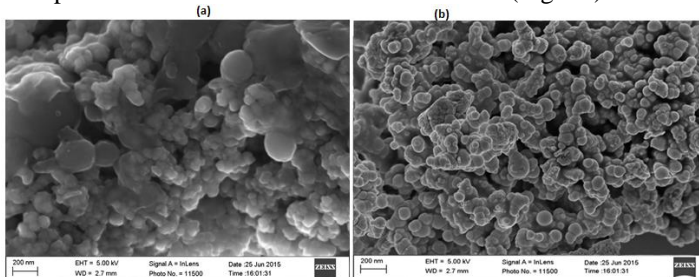


Figure 7: SEM for as-prepared (a) magnetite and (b) magnetite silica NPs

Other studies found that with variation in amount of the TEOS, silica-coated magnetite particles become more monodispersed as a result of the reduction in the relative size distribution and uniform silica-coated magnetite particles formed [15]. The Figure 7b also shows that monodisperse nanoparticles were arranged in a 2-D closed packed way, demonstrating the uniformity of the particle size. These NPs could be well suited for many applications involving its incorporation in nanocomposites fabrication.

The surface modified magnetite NPs using silica nanoparticles had increased stability at room temperature.

This stability is based on creating electrostatic repulsions due to ionic compounds between the NPs that can overcome the magnetic and surface-related attractions. The as-prepared magnetite nanoparticles were negatively charged, resulting in electrostatic repulsion between each particle and thus prevented the nanoparticles from aggregation [16].

*d. POWDER X-RAY DIFFRACTION*

Magnetite (Fe<sub>3</sub>O<sub>4</sub>) nanoparticles synthesized by solvothermal method were examined by X-ray diffractometer (Shimadzu, XRD-6000) equipped with CuK $\alpha$  radiation source using Ni as filter at setting of 30 kV/30 mA (Fig. 8a,b).

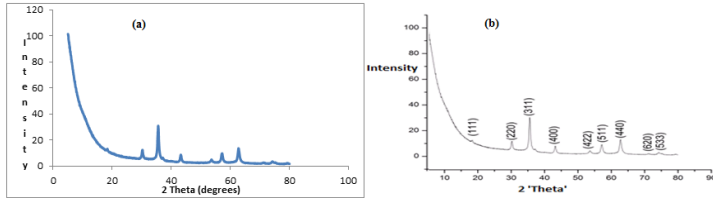


Figure 8: The D(hkl) values for XRD pattern

Figure 8 also shows the complete range of allowed electron transitions in our synthesized magnetite NPs. The most intense peak gives D-value of 311 from the Bragg's law:  $n\lambda = 2d\sin\theta$  which was used in determination of NPs diameter using the Full width at half maximum (FWHM) and the Debye-Scherrer equation. In other words, HWHM is the width of a spectrum curve measured between those points on the y-axis which are half the maximum amplitude. The particle size for the most intense peak at D(311) was determined as 22.4 nm from the Debye-Scherrer modified equation:

$$T = \frac{c\lambda}{B\cos\theta} = \frac{c\lambda}{(B_M^2 - B_S^2)^{1/2} \cos\theta}$$

where T is the crystallite thickness,  $\lambda$  the wavelength of the X-rays (T and  $\lambda$  have the same units),  $\theta$  the Bragg angle, and B is the full-width at half-maximum (FWHM) of the peak (radians) corrected for instrumental broadening. ( $B_M$  and  $B_S$  are the FWHMs of the sample and of a standard, respectively. C = the Scherrer shape factor, corresponding to the value for magnetite.

The peaks indexed as planes (220), (311), (400), (422), (511) and (440) corresponded to a cubic unit cell, characteristic of a cubic spinel structure. Therefore, it was confirmed that the crystalline structure of the prepared magnetite nanoparticles, agreed with the structure of an inverse spinel type oxide. The analysis of the diffraction pattern showed the formation of a cubic spinel structure in the sample; due to the strongest reflection that proceeds from the (311) plane (Fig. 8a, b), characteristic of such a phase [17].

*e. SQUID-MPMS MAGNETOMETRY*

The magnetic behaviour of different magnetic substances is demonstrated by their hysteresis curves in a plot of magnetic flux density, B, against applied magnetic field, H [18]. Based on the hysteresis properties of materials, it is possible to define each of these magnetic characteristics from a mixture of magnetic assemblages. The magnetization curve of our synthesized magnetic Fe<sub>3</sub>O<sub>4</sub>-SiO<sub>2</sub> NPs at room temperature is showed in figure 9a.

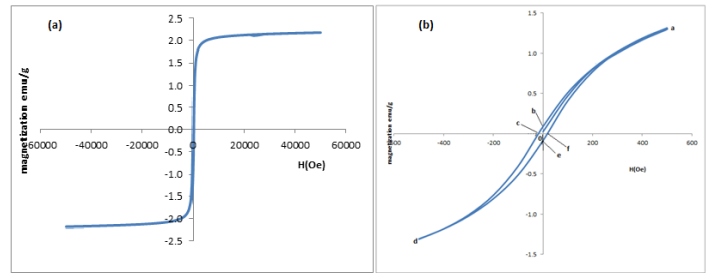


Figure 9: (a) magnetization curve for prepared silica coated magnetite NPs at room temperature. (b) expanded low field region of the hysteresis loop

As the line demonstrates, the greater the amount of current applied, H(Oe); the stronger the magnetic field in the component B(M). A hysteresis loop can be seen although the loop is quite narrow due to multi-domain particles unlike single-domain particle which has broad loop. The difference between ferromagnetic (FM) and superparamagnetic (SPM) behavior is primarily due to the size of the particle. As soon as the size gets small enough, the later takes effect. The as prepared magnetite NPs exhibited a narrow hysteresis loop which confirmed its super-paramagnetic property [19].

From the magnetization behavior, the saturation magnetization (Ms) of the Fe<sub>3</sub>O<sub>4</sub>-SiO<sub>2</sub> NPs increase from 1.50 to 2.0 emu/g. The small particle sizes exhibit smaller values of Ms as expected due to the surface disorder and modified cationic distribution. In other words, the decrease in Ms at smaller sizes is attributed to the pronounced surface effects in these nanoparticles. The surface of the nanoparticles is considered to be composed of some canted or disordered spins that prevent the core spins from aligning along the field direction resulting in decrease of the saturation magnetization of the small sized nanoparticles [20].

Although particles having coercivity less than 20 O<sub>e</sub> are sometime termed as superparamagnetic, these particles saturates at a certain magnetic field similar to ferri and ferro magnetic particles. The only difference between superparamagnetic and ferromagnetic is that the coercivity goes to almost zero in superparamagnetic materials (SPM) while it is appreciable in the case of ferromagnetic materials (FM). If the particle sizes are monodisperse then the coercivity will be zero. In the present study, the magnetization values of 2.0 emu/g is almost equal to that of synthesized MMSP-GO composites which had saturation magnetization of 7.5 emu g<sup>-1</sup> with superparamagnetic properties. This confirms that the as-prepared magnetite-silica NPs have characteristic superparamagnetic properties. This study shows an external field response which followed a sigmoidal curve, a characteristic property of superparamagnetic NPs [21].

C. CHARACTERIZATION OF CNT-IPSF/Fe<sub>3</sub>O<sub>4</sub> NANOCOMPOSITES

*a. SEM-EDS ANALYSIS*

The structure of the membranes was characterized by SEM-EDAX technique. The SEM image of fabricated magnetic CNT-IPSF nanocomposite is shown in Figure 10.

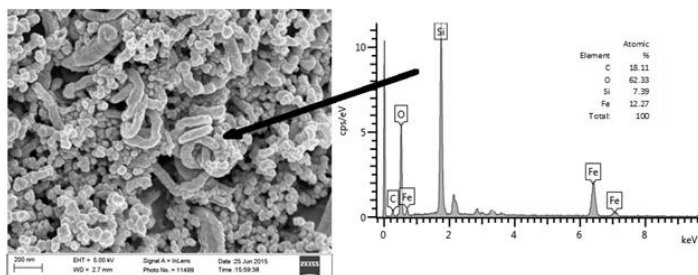


Figure 10: SEM-EDAX analysis for as prepared magnetite CNT-IPSF nanocomposites

From Fig.10, a large quantity of dispersive magnetite NPs having moderately uniform and cubic structures can be seen. The cylindrical needle-like threads of CNTs can be seen interlinking with the magnetite NPs. The SEM of as-prepared Magnetite - CNT revealed well packed and uniform structure with higher surface area suitable for adsorption studies. In this study, carbon nanotubes (CNTs) were sonicated with magnetite NPs which altered their mechanical properties through thorough mixing. In addition, such process also increases the number of defects on the walls of the CNTs; breaking inertness and enhancing reactivity [22]. Chemical analysis from EDS (inset) confirms the presence of Fe and O elements. With the stoichiometry  $\text{Fe}_3\text{O}_4$  phase, the presence of C and S confirms the inclusion of CNTs and infused polysulfone respectively into the membrane.

#### b. TEM Analysis

The TEM analysis of the membrane in Figure 11 confirms the presence of spherical magnetite NPs interlinking the long threadlike CNTs.

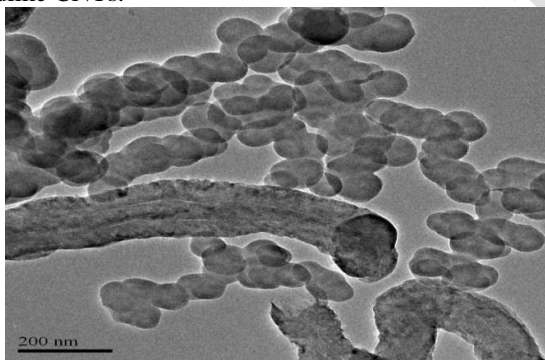


Figure 11: TEM for as prepared CNTs-IPSF/ $\text{Fe}_3\text{O}_4$  nanocomposites

#### IV. CONCLUSIONS

The CNT-IPSF/ $\text{Fe}_3\text{O}_4$  nanocomposites were successfully fabricated from CNT-IPSF polymer and  $\text{SiO}_2\text{-Fe}_3\text{O}_4$  nanoparticles based on various characterization procedures. The synthesized CNTs by CVD process at 600 °C had threadlike twisting and winding entities for multiwalled CNTs from SEM characterization with its TEM showing average internal diameters of 40-50 nm.

Magnetite NPs prepared by solvothermal process and the silica-coated magnetite NPs by modified Stöber method exhibited UV-Vis spectra with broad absorption peaks at

wavelength at about 396 nm and 395 nm which resulted in band gap energies of 3.14 eV and 3.13 eV respectively confirming stabilization of NPs upon coating with silica. The presence of absorption band between 480  $\text{cm}^{-1}$  and 580  $\text{cm}^{-1}$  in the IR spectrum was assigned to the vibrations of Fe-O bond confirming the formation of  $\text{Fe}_3\text{O}_4$  nanoparticles. The SEM image revealed that the formation of magnetite-silica nanoparticles which were monodispersed.

XRD analysis revealed magnetite silica NPs with peaks indexed as planes (220), (311), (400), (422), (511) and (440) corresponded to a cubic unit cell, characteristic of a cubic spinel structure due to the strongest reflection that proceeds from the (311) plane, characteristic of such a phase. Crystallite size measurements were determined as 22.4 nm from the strongest reflection of the (311) peak, using the Scherrer approximation, which assumes the small crystallite size to be the cause of line broadening. Also, no characteristic peaks of impurities were observed.

The magnetization behavior determined by SQUID-MPMS magnetometer did display very narrow hysteresis loop and zero coercivity was detected from the curve. This distinguished it from ferromagnetic material that has hysteresis loops for its particles and which are narrower about the origin than antiferromagnetic loops. The external field response of these NPs followed a sigmoidal curve with saturation magnetization of 2.2  $\text{emu g}^{-1}$  characteristic of superparamagnetic material. This would ensure effective magnetoresponsive separation after adsorption equilibrium. The SEM for as-prepared PSF-CNT/ $\text{Fe}_3\text{O}_4$  nanocomposite further revealed well packed and uniform structure depicting higher surface area suitable adsorption studies.

#### REFERENCES

- [1] Armentano, I., et al., *Biodegradable polymer matrix nanocomposites for tissue engineering: a review*. Polymer degradation and stability, 2010. 95(11): p. 2126-2146.
- [2] Tanahashi, M., *Development of fabrication methods of filler/polymer nanocomposites: With focus on simple melt-compounding-based approach without surface modification of nanofillers*. Materials, 2010. 3(3): p. 1593-1619.
- [3] Rafatullah, M., et al., *Adsorption of methylene blue on low-cost adsorbents: a review*. Journal of hazardous materials, 2010. 177(1): p. 70-80.
- [4] Tiraferri, A., et al., *Superhydrophilic thin-film composite forward osmosis membranes for organic fouling control: fouling behavior and antifouling mechanisms*. Environmental science & technology, 2012. 46(20): p. 11135-11144.
- [5] Mathew, D.S. and R.-S. Juang, *An overview of the structure and magnetism of spinel ferrite nanoparticles and their synthesis in microemulsions*. Chemical Engineering Journal, 2007. 129(1): p. 51-65.
- [6] Wu, W., Q. He, and C. Jiang, *Magnetic iron oxide nanoparticles: synthesis and surface functionalization strategies*. Nanoscale Research Letters, 2008. 3(11): p. 397.

- [7] Kumar, M., & Ando, Y. . *Chemical vapor deposition of carbon nanotubes: a review on growth mechanism and mass production*. Journal of nanoscience and nanotechnology, 2010. 10(6): p. 3739-3758.
- [8] Wakeman, R. and C. Williams, *Additional techniques to improve microfiltration*. Separation and Purification Technology, 2002. 26(1): p. 3-18.
- [9] Deng, Y., et al., *Superparamagnetic high-magnetization microspheres with an Fe<sub>3</sub>O<sub>4</sub>@ SiO<sub>2</sub> core and perpendicularly aligned mesoporous SiO<sub>2</sub> shell for removal of microcystins*. Journal of the American Chemical Society, 2008. 130(1): p. 28-29.
- [10] Gohil, J. and P. Ray, *Polyvinyl alcohol as the barrier layer in thin film composite nanofiltration membranes: Preparation, characterization, and performance evaluation*. Journal of colloid and interface science, 2009. 338(1): p. 121-127.
- [11] Pierard, N., et al., *Production of short carbon nanotubes with open tips by ball milling*. Chemical Physics Letters, 2001. 335(1): p. 1-8.
- [12] Lahure, *Preparation and Characterization of Magnetite Nanoparticle using Green Synthesis*. International Journal of Research in Chemistry and Environment, 2015. 5(4): p. 38-43.
- [13] Kulkarni, S.A., P. Sawadh, and P.K. Palei, *Synthesis and Characterization of Superparamagnetic Fe<sub>3</sub>O<sub>4</sub>@ SiO<sub>2</sub> Nanoparticles*. J. Korean Chem. Soc, 2014. 58.
- [14] Ngo, T.H., et al., *Facile and solvent-free routes for the synthesis of size-controllable Fe<sub>3</sub>O<sub>4</sub> nanoparticles*. Advances in Natural Sciences: Nanoscience and Nanotechnology, 2010. 1(3): p. 035001.
- [15] Zhao, W., et al., *Fabrication of uniform magnetic nanocomposite spheres with a magnetic core/mesoporous silica shell structure*. Journal of the American Chemical Society, 2005. 127(25): p. 8916-8917.
- [16] Wei, X., et al., *A novel method of surface modification to polysulfone ultrafiltration membrane by preadsorption of citric acid or sodium bisulfite*. Memb. Water Treat, 2012. 3: p. 35-49.
- [17] Lopez, J.A., et al., *Synthesis and characterization of Fe<sub>3</sub>O<sub>4</sub> magnetic nanofluid*. Revista Latinoamericana de Metalurgia y Materiales, 2010: p. 60-66.
- [18] Chen, C.-W., *Magnetism and metallurgy of soft magnetic materials* 2013: Courier Corporation.
- [19] Gass, J., et al., *Superparamagnetic polymer nanocomposites with uniform Fe<sub>3</sub>O<sub>4</sub> nanoparticle dispersions*. Advanced Functional Materials, 2006. 16(1): p. 71-75.
- [20] Maaz, K., et al., *Synthesis and magnetic characterization of nickel ferrite nanoparticles prepared by co-precipitation route*. Journal of magnetism and magnetic materials, 2009. 321(12): p. 1838-1842.
- [21] Kolhatkar, A.G., et al., *Tuning the magnetic properties of nanoparticles*. International journal of molecular sciences, 2013. 14(8): p. 15977-16009.
- [22] Ayala, P., et al., *The doping of carbon nanotubes with nitrogen and their potential applications*. Carbon, 2010. 48(3): p. 575-586.